Chapter

In-Liquid Plasma: A Novel Tool for Nanofabrication

Palash Jyoti Boruah, Parismita Kalita and Heremba Bailung

Abstract

This chapter focuses on synthesising nanomaterials using an emerging technology called In-Liquid Plasma, i.e., plasma generation inside a liquid. The generation of various reactive species and energetic electrons in the plasma zone plays a crucial role in synthesising nanomaterials. They act as the reducing agent. Non-requirement of the toxic chemical reducing agents make In-Liquid Plasma an environmentally friendly green approach to fabricate nanomaterials. This method enables the simultaneous synthesis of nanoparticles from the electrode material and liquid precursor, which gains much importance on the single-step synthesis of nanocomposites. Moreover, it gives flexibility in controlling both the physical and chemical parameters, which provide fine-tuning required for the size, shape and composition of nanomaterials.

Keywords: In-Liquid Plasma, Plasma zone, Reactive species, Nanomaterial, Precursor solution, Size and shape transformation

1. Introduction

Plasma technology has been involved in various biomedical and environmental applications for quite a long time. From the treatment of cancer to the polluted water, its involvement increases day by day to humankind. Moreover, plasma has also been immensely engaged in the fabrication of high-quality nanomaterials [1]. Various methods have been employed to generate the plasma both in the non-thermal and thermal conditions. Amongst them, Plasma – Liquid Interaction (PLI) gains a lot of attention as it involves both the physical and chemical processes simultaneously [2]. It offers single-step, rapid and large-scale synthesis of uniform nanomaterials with different shapes and sizes [3]. One of the advantages of PLI is that it does not require any external reducing and stabilising chemical agents, so a few purification steps can be avoided before applying in any application. The reactive species form during the generation of plasma act as the reducing or oxidising agents. Moreover, it does not require water cool vacuum chambers or pumping systems. PLI offers two effective ways for nanomaterial synthesis. The first one is from the electrode material by generating plasma between two electrodes placed in a liquid. This process is termed as In-Liquid Plasma or solution plasma. Here, nanomaterials can also synthesised using specific metal precursor solutions. Hence, both the electrode material and the precursor solution can be the source of nanomaterial formation. In the second one, nanomaterials are fabricated by generating plasma above a liquid surface. Here, one electrode is placed above the

liquid surface and the other is immersed into the liquid in such a way that the liquid surface acts as the counter electrode. The liquid (precursor) acts as the nanomaterial source i.e., plasma interact with the liquid solution to synthesise nanomaterials.

In-Liquid Plasma mainly consists of three zones. The central zone is the plasma region, where the temperature goes beyond thousands of kelvin. The next one is the gaseous region, which is formed due to the evaporation of water/solvent. The outermost zone is the liquid medium, where the temperature is slightly more than the room temperature. Besides these zones, there are two interfacial regions called the plasma/gas and gas/liquid interface. These are very significant regions for nanomaterial synthesis, where many physical and chemical activities occur. A broad range of active radicals such as OH^*, H_2O_2, O_3, NO, $e^-_{(aq)}$, UV radiations and shock waves are formed in these interfacial zones [4]. **Figure 1** shows the presence of the three zones (plasma, gas and liquid) and the interfacial regions (plasma/gas and gas/liquid) during the generation of plasma inside a liquid. This chapter will mainly discuss the In-Liquid Plasma, i.e., plasma generation inside liquid to synthesise various nanomaterials. A review of nanofabrication by In-Liquid Plasma over the last two decades has been discussed in the following paragraphs.

Since the beginning of the 21st century, In- Liquid Plasma has been vigorously involved in the synthesis of various nanomaterials. In the early years, researchers have mainly focused on the synthesis of carbon-based nanomaterials [5–8]. In 2000, Ishigami et al. reported the continuous synthesis of multi-walled carbon nanotubes by generating arc discharge between two graphite electrodes inside liquid nitrogen [5]. Whereas Sano et al. in 2001 investigated the synthesis of carbon onions in water [6] and in 2004, single-walled carbon nanotubes with nanohorns in liquid nitrogen [9]. Bera et al. synthesised palladium nanoparticles filled carbon nanotubes using arc discharge in palladium chloride ($PdCl_2$) solution in 2004 [10]. After these pioneering investigations, researchers began to work on the synthesis of noble and

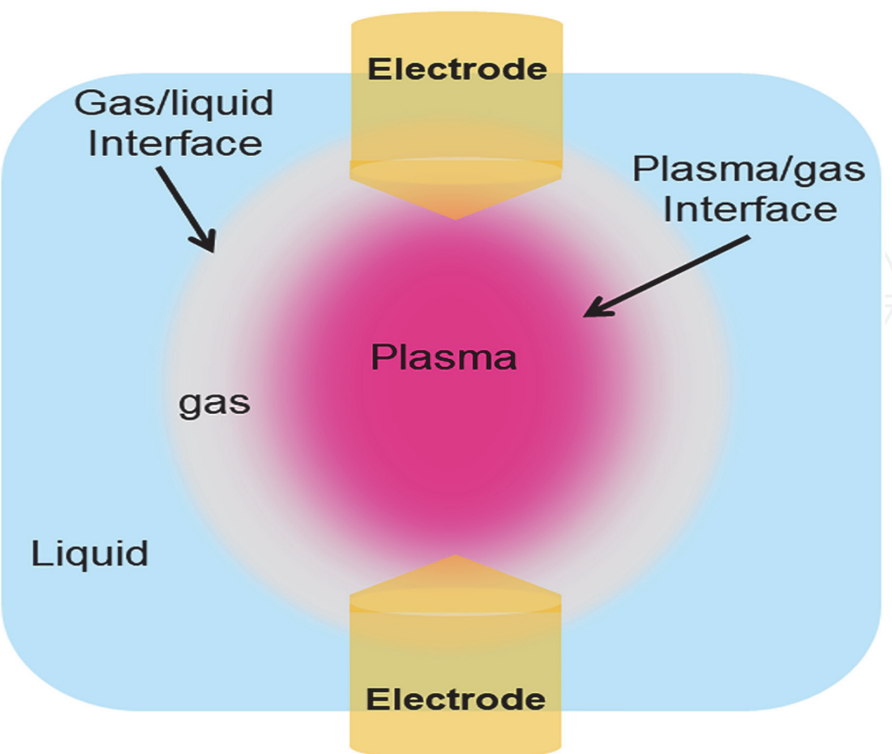

Figure 1.
Schematic representation of the generation of plasma inside a liquid showing the presence of plasma/gas and gas/liquid interfaces.

transition metal nanomaterials and their composites. Lo et al. synthesised Copper (Cu) – based nanofluids and silver nanofluids using submerged arc nanoparticle synthesis system (SANSS) in 2005 and 2007 respectively [11, 12]. Lung et al., in 2007, reported the synthesis of gold (Au) nanoparticles in water by arc discharge [13]. Ashkarran et al. synthesised tungsten trioxide (WO_3), Zinc oxide (ZnO) and Zirconium oxide (ZrO_2) nanoparticles inside water in 2008 [14], 2009 [15] and 2010 [16] respectively. In 2009, Omurzak et al. reported the synthesis of blue amorphous titanium oxide (TiO_2) and Ti_nO_{2n-1} nanoparticles by generating plasma between two titanium electrodes [17].

In the meantime, besides the erosion of electrode materials, the researchers investigated the reduction of metallic salt solutions by the In-Liquid Plasma for the synthesis of various nanomaterials. Saito et al., in 2009, synthesised Au nanoparticles by generating plasma between two tungsten electrodes inside Chloroauric acid ($HAuCl_4$) [18]. $HAuCl_4$ acts as the metal precursor for Au nanoparticles. Pootawang et al. investigated the synthesis of silver/platinum (Ag/Pt) bimetallic nanocomposites by producing plasma between a silver and a platinum electrode inside a mixture of solution containing sodium dodecylsulfonate (SDS) and sodium chloride (NaCl) using a unipolar pulse power supply in 2012 [19]. Synthesis of WO_3, Ag and Au nanoparticles by generating plasma between a metal electrode (tungsten or silver or gold) and a copper plate was investigated by Hattori et al. in 2013 [20]. Lee et al., in 2014, synthesised tin (Sn) and tin oxide (SnO_2) nanoparticles by the reduction of tin chloride dehydrate ($SnCl_2.\ 2H_2O$) [21]. Fabrication of manganese (Mn) oxide/activated carbon composites was investigated by Lee et al. in 2015 [22]. They used a mixture of manganese chloride tetrahydrate ($MnCl_2.4H_2O$) and activated carbon powder as the solution. The former and latter act as the precursor for manganese oxide and carbonaceous material respectively. Synthesis of bimetallic Nickel (Ni)/Copper (Cu) nanoparticles by generating plasma inside a mixture of nickel nitrate hexahydrate ($Ni(NO_3)_2.6H_2O$) and copper nitrate tetrahydrate ($Cu(NO_3)_2.4H_2O$) solution was reported by Sun et al. in 2016 [23]. To enhance catalytic activity towards oxygen reduction reaction (ORR), Panomsuwan et al. reported the synthesis of metal-free composite of nitrogen-doped carbon nanoparticles (NCNP)/carbon nanofiber (CNF) using solution plasma in 2016 [24]. The composites were obtained by generating plasma inside a mixture of CNF and 2 – cyanopyridine ($C_6H_4N_2$), where the latter act as the source of nitrogen. Fabrication of bead-chain-like nanostructures of ZnO from the oriented attachment of spherical Zn/ZnO nanoparticles by generating DC plasma between two Zinc electrodes inside deionised water was reported by Ziashahabi et al. in 2017 [25]. Fabrication of nitrogen-doped activated carbon-supported iron oxide (Fe_2O_3) nanocomposites for supercapacitor applications was investigated by Lee et al. in 2018 [26]. They first prepared the nitrogen-doped carbon (NC) by Liquid Phase Plasma (LPP) inside a solution containing ammonium chloride (NH_4Cl) and activated carbon (AC) powder, where the former act as the precursor for nitrogen. After that, the resultant particles were mixed in iron chloride ($FeCl_2$) and Cetyltrimethyl ammonium bromide (CTAB) solution. The LPP reaction then gives the iron oxide/NC composites (IONCC). The specific capacitance and cyclic stability of NC and IONCC were found superior to the bare AC. Synthesis of Cu – Ni/CuO – NiO (CNO) nanocomposites by generating a plasma between a copper and nickel electrodes inside water using a bipolar pulse high voltage power supply was reported by Yang et al. in 2020 [27]. They found superior catalytic activity of CNO towards methanol electrocatalytic oxidation in alkaline media than the other transition metal or metal oxide based catalyst. Boruah et al. in 2021, reported a novel single-step synthesis method of Au/CuO micro/nanocomposites by generating plasma between two copper electrodes inside a solution of $HAuCl_4$ [28]. The

copper electrodes acted as the source of CuO particles and the $HAuCl_4$ acted as the precursor of Au nanoparticles.

Moreover, researchers have also focused on the fabrication of nanomaterials having various defect states to enhance the catalytic activity of the materials during the last few years. Panomsuwan et al., in 2015, reported the synthesis of defect-induced black titanium oxide (H-TiO_{2-x}) nanoparticles by generating plasma between two titanium electrodes inside water [29]. They observed a higher photocatalytic performance of H-TiO_{2-x} (90%) than the commercial TiO_2 particles (18%) for the degradation of Methylene blue (MB) dye under visible light irradiation. Moreover, about 51% of MB molecules adsorbed on the surface of H-TiO_{2-x} under dark, whereas for commercial TiO_2, the adsorption was about only 9%. The same group in 2018 fabricated defect–induced heterophase anatase/brookite TiO_{2-x} nanocrystals by generating plasma inside a solution containing commercially available TiO_2 powder [30]. Active radicals present in the plasma interact with the TiO_2 particles to form defective sites. A higher gaseous photocatalytic activity towards acetaldehyde degradation to CO_2 of the plasma-treated particles (TiO_{2-x}) (91.1%) than the untreated commercial TiO_2 particles (51%) was observed. Boruah et al. in 2020 synthesised narrow bandgap tungsten oxide (WO_{3-x}) nanoparticles by generating plasma inside deionised water [31]. The reason behind the formation of narrow bandgap nanoparticles was investigated to be the presence of higher amount of oxygen vacancies. They observed higher photocatalytic performance of WO_{3-x} nanoparticles (77%) than the commercial nano WO_3 (62%) and bulk WO_3 (50%) particles under a solar simulator.

2. Experimental details and methodology

2.1 Experimental designs

The design of experimental setups mainly depends on two electrode configurations: pin-to-pin and pin-to-plane. In the first one, two pointed electrodes are placed vertically towards each other and in the second one, a pointed electrode is positioned vertically to a planar (plate) electrode. The advantage of pin-to-pin and pin-to-plane electrode configuration is to attain maximum electric field at a desired electrode gap. Various types of voltage waveforms such as DC, pulsed DC, AC, RF (radio-frequency) and microwave are used to generate plasma. **Figure 2** (a) and (b) shows the generation of plasma using the pin-to-plane and pin-to-pin electrode configurations respectively, in our laboratory. For pin-to-plane, it is observed that

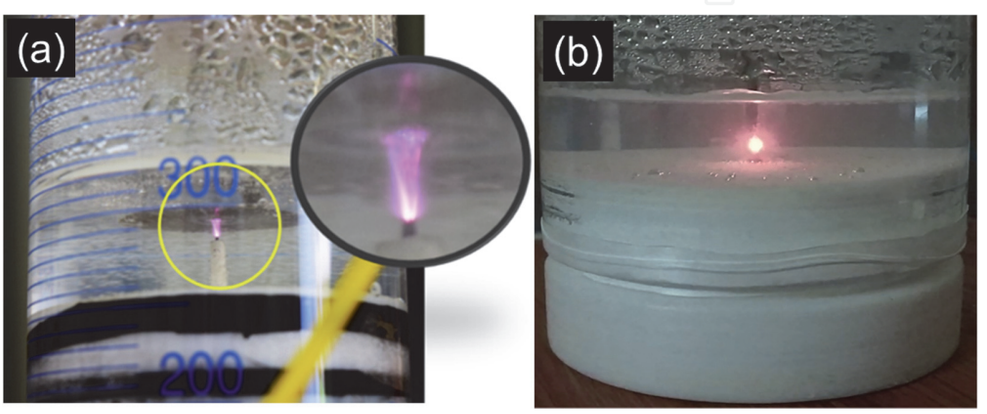

Figure 2.
Generation of plasma using (a) pin-to-plane and (b) pin-to-pin electrode configurations.

the plasma channel diverse from the pin electrode towards the plane electrode and for pin-to-pin, the plasma expands at the central region from the tip of the two electrodes. Hattori et al. employed a pin-to-plane electrode configuration to generate a plasma between a metallic electrode and a copper plate using radio-frequency plasma [20]. Whereas Lange et al. reported the use of pin-to-pin electrode configuration to generate a plasma between two vertically pointed graphite electrodes using a DC power supply [8].

Many different types of experimental setups have been designed so far for the fabrication of nanomaterials in various liquids. Ishigami et al. designed the experimental setup for the continuous production and transportation of carbon nanotubes [5]. They dipped a graphite anode and a short copper or graphite cathode having pin-to-pin electrode geometry into a vessel containing liquid nitrogen. After the generation of plasma, carbon nanotubes were formed due to the erosion of the anode material. They made funnel-shaped bottom of the vessel and sealed it with a valve to operate continuously. The valve opens periodically to transfer the nanotubes from the vessel. In a pin-to-pin or pin-to-plane electrode configuration, erosion of anode is much higher than the cathode erosion [32]. Hence, the resultant nanomaterial is made of anode material.

2.2 Mechanism of plasma generation

Usually, a pulsed high voltage power supply with a voltage rise time shorter than the Maxwellian relaxation time of the liquid is required to generate plasma inside a liquid [33]. When a high voltage is applied between the two electrodes inside a liquid, it induces a current and redistribution of the electric field. Subsequently, Joules heating at the tip of the electrodes takes place, which initiates the bubble formation due to the evaporation of the liquid. Eq. (1) provides an expression for the theoretical maximum of the electric field in pin-to-plane electrode configuration [34]:

$$E_m = \frac{2V_i}{Rln(2D/R)} \tag{1}$$

Where, V_i, R and D represent the applied voltage, the radius of curvature of the pin electrode tip and the distance between the two electrodes respectively. Therefore, to attain the maximum electric field (E_m) at a constant voltage, both the radius of curvature of the pin electrode tip and the distance between the two electrodes should be as minimum as possible. When the applied voltage is increased to a specific value, the high electric field initiates the discharge inside the bubbles. When the bubbles are bridged together, a continuous plasma channel is formed between the two electrodes. The formation of plasma or the conductive channel depends on the Joules heating. When it is larger than a threshold value, instability occurs, which stimulates the immediate evaporation of the liquid followed by thermal breakdown. Hence, plasma is generated between the two electrodes. However, when Joules heating is smaller than the threshold value, only electrolysis takes place. The mechanism of plasma discharge inside liquid also depends on its polarity. As water is a polar medium, it can conduct current and the plasma discharge occurs using the mechanism as explained above. However, for a non-polar medium, the discharge mechanism is slightly different. As non-polar medium cannot conduct electricity hence, bubble formation does not take place. Therefore, plasma generation can only be possible when the electric field between the two electrodes is high enough to trigger the dielectric breakdown of the medium. The dielectric breakdown can be defined as the sharp reduction in the electric resistance of a medium,

when the electric field is higher than the dielectric constant of the medium. Li et al. compared the mechanism of plasma discharge in polar (tap water) and non-polar (benzene) solution [35]. The dielectric constant of benzene is $\sim 10^6$ V/m. They observed the discharge inside benzene after applying the voltage between the two electrodes (electrode gap 0.5 mm) reached 1.5 kV. However, for tap water, the plasma discharge channel was observed by applying less than 1 kV.

2.3 Plasma diagnostics and influence of reactive species on material fabrication

As the plasma inside the liquid is confined to a tiny region, spectroscopic diagnostics is mainly employed to determine the plasma parameters such as plasma density and temperature. Optical emission spectroscopy (OES) helps to identify the presence of various reactive species in the plasma zone. The emission spectrum obtained from the plasma zone is the superposition of the continuous spectra of electron radiation and band or line spectra of various molecules, atoms and radicals. Stark broadening of spectral lines and line intensity ratios are employed to determine the plasma density and temperatures respectively [36]. The temperature of the plasma zone is very crucial to fabricate various nanoparticles from the electrode materials. When two or more spectral lines of the same element (atom or ion) are present in the emission spectrum, then the electron/excitation temperature of the plasma from the line intensity ratio can be expressed as [37].

$$T_e = \frac{E_2 - E_1}{k \ln\left(\frac{I_1 A_2 g_2 \lambda_1}{I_2 A_1 g_1 \lambda_2}\right)} \tag{2}$$

Where, subscripts 1 and 2 denote two different spectral lines of the same element. I, E, A, λ, g, and k are the relative intensity, the energy of upper level, transition probability, the wavelength of the emission line, statistical weight and Boltzmann constant respectively. When the temperature exceeds the boiling point of the electrode material, there is a high probability of the vaporisation of the electrode material to form the nanoparticles. Dunleavy et al. observed the presence of two well-defined regions of plasma [38]. A central core having high temperature $\sim (16000 \pm 3500)$ K with high electron density $N_e \sim 5 \times 10^{17}$ cm^{-3}. The region is at local thermodynamic equilibrium (LTE). As for LTE, the minimum electron density is 2×10^{17} cm^{-3}. The other is the low density ($N_e \sim 10^{15}$ cm^{-3}) peripheral region, which is much cooler having temperature ~ 3500 K. In a unique work of deposition of anti-corrosion layer using plasma electrolytic carbonitriding on pure aluminium, the electron density and temperature were calculated to be 6×10^{15} cm^{-3} and 4000 K respectively [39].

The generation of various reactive species such as hydrogen (H^*), oxygen (O^*), hydroxyl (OH^*) and superoxide (O_2^{*-}) radicals in the plasma region can be explained using the following reactions [2]:

$$H_2O + e^- \rightarrow 2H^* + O^* + e^- \tag{3}$$

$$H_2O + e^- \rightarrow H^* + OH^* + e^- \tag{4}$$

$$O^* + O^* \rightarrow O_2 \tag{5}$$

$$H^* + O_2 \rightarrow HO_2^* \leftrightarrow O_2^{*-} + H^+ \tag{6}$$

During the formation of metal nanoparticles from the electrolytic solution, the expression for the reduction of metal ions (M^{n+}) dissolved in the solution by energetic electrons in the plasma zone is as follows:

$$M^{n+} + ne^- = M \tag{7}$$

The mechanism of the formation of Au nanoparticles using the gold precursor solution ($HAuCl_4$) can be understood by considering the Eqs. (8)-(12) reported by Ashkarran et al. [40] and Bratescu et al. [41]. Here $0 < j < 4$ and the replacement of Cl^- by OH^- depends on the pH of the solution.

$$HAuCl_4 \rightarrow H^+ + AuCl_4^- \tag{8}$$

$$AuCl_4^- + 3e^- \rightarrow Au^0 + 4Cl^- \tag{9}$$

$$AuCl_4^- + jOH^- \leftrightarrow AuCl_{4-j}^-(OH)_j^- + jCl^- \tag{10}$$

$$AuCl_4^- + 3H^* \rightarrow Au^0 + 4Cl^- + 3H^+ \tag{11}$$

$$Au(OH)_4^- + 3H^* \rightarrow Au^0 + OH^- + 3H_2O \tag{12}$$

Klapkiv et al. reported a simulation study on the synthesis of Al_2O_3 by considering the plasma channel into three zones [42]. In the central zone of the plasma channel, the temperature ranges from 7000 to 10000 K and the density of electrons in the order of 10^{22} cm^{-3}. Here, the evaporated anodic materials (made of aluminium, Al) are partially ionised and all the other species are in a monoatomic state. In this zone, Al reacts with singlet oxygen to form AlO, Al_2O, and AlO_2 as given by the following reactions:

$$Al + O \leftrightarrow AlO \tag{13}$$

$$2Al + O \leftrightarrow Al_2O \tag{14}$$

$$Al + 2O \leftrightarrow AlO_2 \tag{15}$$

In the next zone, the temperature is about 5400 K and the reactive molecular species can exist. The following reactions are possible in this zone:

$$Al + OH \leftrightarrow AlO + \tfrac{1}{2}H_2 \tag{16}$$

$$2Al + OH \leftrightarrow Al_2O + \tfrac{1}{2}H_2 \tag{17}$$

The temperature of the third zone is around 2327 K and the formation of Al_2O_3 is possible using the following equations:

$$2Al + 3O \leftrightarrow Al_2O_3 \tag{18}$$

$$2AlO + O \leftrightarrow Al_2O_3 \tag{19}$$

$$Al_2O + 2O \leftrightarrow Al_2O_3 \tag{20}$$

$$2Al + 3OH \leftrightarrow Al_2O_3 + \tfrac{3}{2}H_2 \tag{21}$$

After this region, the temperature of the liquid medium falls to around 300 K (room temperature of the liquid). During this drastic temperature change, the polymorphic transition in the oxide phases is possible.

Optical Emission Spectroscopy also provides the emission spectra of electrode materials; therefore, one can get an idea about the formation of nanoparticles from the electrode material before going through the other material characterisation techniques. To detect the plasma species, Lu et al. used OES, where they observed the emission of Cu atoms along with the other plasma species such as OH, H_α, H_β, O and Na [43]. From the emission of Cu atoms, they suggested that at first, copper foil anode is oxidised to form Cu^{2+}, which then move towards the cathode due to the

external electric field inside the plasma region. During their movement, they react with high-energy electrons and H atoms to form Cu atoms. As copper atoms are highly reactive in water, they are easily oxidised to form CuO nanoparticles. However, Saito et al. reported the synthesis of CuO nanoflower by considering a slightly different mechanism [44]. Firstly, copper hydroxide [$Cu(OH)_2$] is formed at the surface of the copper electrode. The temperature of the electrolyte covering the electrode goes beyond 260°, which is sufficient to melt the surface of the electrode. Secondly, $Cu(OH)_2$ interacts with plasma-generated OH^- to form tetrahydroxocuprate(II) anions $[Cu(OH)_4]^{2-}$. Lastly, as the temperature drops, precipitation of CuO (s) occurs by releasing H_2O and OH^-. Preferential growth of crystal plane along with a specific direction forms spindle structures.

3. Synthesis of nanomaterials by controlling process parameter

It is well known that nanoparticles have widespread applications in various field such as solar cells, photo-thermal cancer treatment, controlled drug delivery, catalysis etc., because of its tunable optical, electrical and catalytic properties which strictly depends on its structure and morphology of the particle. Therefore, nowadays, researchers have devoted substantial effort to have proper control on the shape and size of nanoparticles by simply controlling the fundamental physical and chemical parameters. One of the main advantages of In-Liquid Plasma method for nanofabrication is that it provides flexibility in controlling both the physical (plasma) as well as the chemical (solution) parameters. However, in the chemical-based synthesis, only solution parameters and in the gas phase plasma synthesis of nanomaterial, only plasma parameters can be controlled. Process parameters have a very significant role in the morphology and composition of nanomaterials.

3.1 Variation of physical parameters

In the plasma – liquid interface, due to the interaction of energetic electrons with the liquid medium, various reactive species are formed, which play a significant role as the reducing agent in nanomaterial synthesis. Interestingly, these plasma-generated reducing agents are directly related to the discharge voltage and current applied to generate plasma. Therefore, the proper understanding of the role of discharge voltage and current on nanomaterial synthesis is very essential. Saito et al. investigated the size of Au nanoparticles by varying the discharge voltage [18]. For the applied voltage of 1600 and 3200 V, after 1 min of plasma discharge, dendrite shape nanoparticles of size ~150 nm and after 5 min of discharge ~50 nm nanoparticles were observed. After 20 mins of discharge, for 1600 V applied voltage, a slight change of the size of the nanoparticles was observed. However, for 3200 V applied voltage, the particle size decreased significantly with some anisotropic shapes such as triangular, pentagonal and hexagonal. After 45 mins of discharge, the size of the nanoparticles reduced up to 20 nm. During the experiment, they also observed that the pH of the solution ($HAuCl_4$) decreased with the increase of discharge time. The change in pH explains the formation small nanoparticles. At low pH, gold nanoparticles dissolve and the reduction rate of gold ion decreases, which leads to a reduction in nanoparticle size and formation of exotic or anisotropic shapes. Ashkarran et al. reported the effect of discharge current on the size of Zirconium oxide (ZrO_2) nanoparticles [16]. For 10 A and 20 A arc current, the average size (diameter) of the spherical particles were 21 nm and 42 nm respectively, i.e. size of the particles increased with the increase in discharge current. As the smaller particles have a larger specific surface area, therefore, they observed

higher photocatalytic activity of the nanoparticles synthesised at lower discharge current. However, Ziashahabi et al. reported contradictory results, where they observed a decrease in the size of the Zn/ZnO nanocomposites with the increase of discharge current [25]. By maintaining the discharge current at 20, 50, 100 and 150 A, the diameter of the particles was 60, 40, 35 and 26 nm respectively. They also observed that the shape of the nanoparticles changed from spherical to bead-like at higher discharge current. For 50, 100 and 150 A discharge current, the length of bead-like aggregates was 114, 117 and 120 nm respectively. Therefore, with the increase in discharge current, the size of nanoparticles decreased in diameter and increased in length. Jin et al. observed the effect of discharge voltage on the shape and size of Ag nanoparticles [45]. To investigate the phenomenon, they fixed the other physical and chemical parameters such as pulse frequency, pulse width, discharge duration, electrode gap and solution concentration at 20 kHz, 2 μs, 600 s, 1 mm and 0.5 mM respectively. When the discharge voltage was in the range of 800–900 V, the particles formed were mostly aggregated and had some dendritic structures. Further increase in discharge voltage to 1000 V, only dendritic structure was observed. This change in morphology of the Ag nanoparticles at higher voltage has been explained by considering the orbit – limiting charging model [46]. The model relates the particle charge with the surface potential as:

$$Q = C\Phi_s \tag{22}$$

Where, Q, C and Φ_s represents the charge, capacitance of the particle in plasma and the surface potential of the particle respectively. As the quantity of electrons is directly proportional to the particle charge. Therefore, when the discharge voltage increases, the generation of energetic electrons also increases, generating more charged particles. A considerable number of electrons surrounds the surface of these charged particles. Hence, further reduction of the Ag ion will take place quite quickly on the already nucleated negatively charged particle, which helps in forming a dendrite structure. They also investigated the effect of nanoparticle morphology by controlling the discharge duration. They also studied the impact on the morphology of the nanoparticles by varying the discharge duration and keeping the applied voltage at 1000 V. At 120 s of discharge duration, nearly spherical Ag nanoparticles of size 12.7 ± 4.4 nm in diameter were observed. When the duration was increased to 500 s, aggregated nanoparticles of a dendritic shape having branch of size 61.8 ± 21.8 nm was observed. However, further increase in discharge duration to 600 s showed an abrupt increase in the size of the dendritic structure to 153.8 ± 54.6 nm. Moreover, during the experiment, they observed the rise of solution temperature from 333 to 368 K. From this observation of temperature rise, they explained the change of morphology of the nanoparticles by considering the Brownian motion of the particles. The below equation is used to explain the relationship between the temperature and the Brownian motion of the nanoparticles:

$$D = kT/6\pi\eta r \tag{23}$$

Where, D, k, T, η and r represents the diffusion constant of particle, Boltzmann constant, temperature, viscosity and radius of particle respectively. Since, along with the discharge duration, the temperature of the solution increased. Therefore, the average kinetic energy of the nanoparticles also increases, which helps in aggregating the particles, due to continuous encounters with each other.

Sun et al. observed the variation on Ni – Cu bimetallic nanoparticle size and shape as well as the percentage of metal components with the plasma discharge duration [23]. With the increase of discharge duration, the size of the nanoparticles

was observed to increase. At the initial stage of discharge, spherical bimetallic nanoparticles and after longer plasma treatment time flower-shaped nanoparticles were observed. Moreover, they observed higher copper content in the bimetallic particles. The atomic composition of the resulting bimetallic nanoparticles was 60% Cu, 30% Ni and 10% Oxygen. The observation can be explained by considering the standard potentials of copper and nickel, as shown by the following equations.

$$Cu^{2+}(aq) + 2e^{-} \rightarrow Cu(s) E^{0} = +0.34V \quad (24)$$

$$Ni^{2+}(aq) + 2e^{-} \rightarrow Ni(s) E^{0} = -0.25V \quad (25)$$

Since, copper has a higher standard potential i.e. lower ionisation tendency than nickel. Hence, copper ions are reduced faster than nickels to have more copper content in the resulting bimetallic nanoparticles. Kang et al. investigated a different phenomenon, where they observed the size and crystallinity of carbon nanospheres by varying the pulse frequency of a bipolar pulse power supply [47]. The voltage, pulse width and electrode gap were controlled at 1.3 kV, 2 μs and 1 mm respectively. Benzene was used as the precursor for carbon nanospheres. By adjusting the pulse frequency from 25 to 65 kHz, the average diameter of the carbon nanospheres was observed to be 20 to 100 nm. Moreover, during the discharge, another interesting phenomenon was observed. When the pulse frequency was adjusted from 25 to 50 kHz, amorphous carbon spheres were synthesised. On the other hand, at 65 kHz, synthesised carbon nanospheres composed continuous short-range graphite with turbostratic structure.

3.2 Variation of chemical parameters

The chemical parameters such as concentration of the solution, pH and use of surfactant plays a significant role in the morphological and chemical compositions of the nanomaterials. In a recent work on the synthesis of Au/CuO micro/nanocomposites, we have reported the shape transformation of CuO particles by simply varying the concentration of the gold precursor ($HAuCl_4$) solution [28]. In the experiment, simultaneously, both the electrode (Cu) and the liquid solution act as the source of materials for the formation of Au/CuO micro/nanocomposites. At low concentration (0.1 mM $HAuCl_4$) of the solution, the shape of CuO was found to be spindle. When the concentration was increased to 0.5 mM, along with the spindle shape, several rod-like structures of CuO were also observed. However, at higher concentration (1 mM), the spindle shape of CuO completely transformed to sheet – like structure. The shape transformation of CuO is believed to be due to the presence of a large number of foreign metal (Au^{3+}) and halide (Cl^{-}) ions at a higher concentration of gold precursor solution. The pH of the gold solution could also be responsible for the shape transformation process. Moreover, with the increase of solution concentration from 0.1 to 1 mM, the size of the Au nanoparticles was found to increase from 7.73 ± 0.11 to 37.50 ± 1.50 nm. A different work reported by Saito et al. investigated the morphology of copper/copper oxide nanoparticles synthesised from the electrode material by varying the concentration of K_2CO_3 solution [44]. They observed the formation of CuO nanoflowers having sharp nanorods, where size increased with increasing the solution concentration. The pH value of the precursor solution also plays a pivotal role in controlling the structure of nanomaterials. In most cases, the pH value of the initial precursor solution is controlled by using different concentrations of NaOH solution. Bratescu et al. investigated the variation of pH on the size of the Au nanoparticles [41]. They used $HAuCl_4.3H_2O$ as the gold precursor. To adjust the pH of the solution, different

amount of NaOH was used. At pH 3, 6 and 12 the average size of the Au nanoparticles was measured to be 10, 4 and 2 nm respectively. They explained the size variation of Au nanoparticles with pH by considering the standard redox potential of Eqs. (11) and (12), which occur at pH 3 and 12 respectively. The standard redox potential of the reduction of $AuCl_4^-$ to Au^0 at pH 3 is 0.95 eV, whereas for $Au(OH)_4^-$ to Au^0 at pH 12 is 0.60 eV [48]. As greater redox potential leads to the formation of a high number of atoms, hence, at pH 3 more number of Au atoms were formed, which aggregates and generate nanoparticles with sizes ~10 nm. At higher pH, less number of atoms were formed, which lead to the formation of smaller Au nanoparticles.

Although most researchers do not use any stabilising agents, a few reported the addition of surfactant to the initial solution. Surfactants mainly act as a capping agent to control the size and shape of the nanoparticles by preventing the aggregation of particles. Kim et al. reported the use of Polyvinylpyrrolidone (PVP) as the stabiliser to observe the size variation of Au nanoparticles at different concentrations [49]. For the experiment, they dissolved 0.1 mM gold precursor $HAuCl_4.3H_2O$ in ethylene glycol. After the plasma discharge, Au nanoparticles with various shapes such as triangular, square and nearly spherical, having sizes 20.85 ± 2.78 nm in diameter and a few nanorods with 10 nm in diameter and 40–45 nm in length, were observed. After that, they mixed potassium chloride (KCl) to generate high plasma density, as potassium ions have higher oxidation potential than hydrogen. For 0.05 and 0.1 M KCl, most of the nanoparticles were observed to be nearly spherical of diameters 17.1 ± 0.48 and 16.38 ± 0.48 nm respectively. Therefore, the use of KCl had a significant role in the shape of the nanoparticles. When 0.01 mM PVP was added to a mixture of 0.05 M KCl and 0.1 mM $HAuCl_4.3H_2O$ solution, the size of the Au nanoparticles was reduced to 12.32 ± 0.87 nm. Moreover, with the increase of the concentration of PVP, the size of the Au nanoparticles decreased and they have a high tendency to become spherical. It indicates that the use of PVP effectively protects the surface of the Au nanoparticles by limiting the crystal growth and results in spherical nanoparticles. Lee et al. reported the effect of a cationic and anionic surfactant on the size of nickel (Ni) nanoparticles [50]. For the cationic and anionic surfactant, Cetyltrimethyl ammonium bromide (CTAB) and Sodium dodecyl sulfate (SDS) respectively were used. Nickel chloride hexahydrate ($NiCl_2.6H_2O$) solution was used as the precursor for Ni nanoparticles. When SDS was added to the solution, formation of spherical nanoparticles at all molar ratios of SDS/$NiCl_2$ were observed. On the other hand, when CTAB was added up to 20% of the molar ratio of CTAB/$NiCl_2$, smaller spherical nanoparticles than the no surfactant case was observed. When the molar ratio was increased to 30% or greater, the formation of large polygonal or whisker-shaped particles was observed. From this experiment, it has been established that cationic surfactant play a significant role in tuning the size and shape of the nanoparticles. Use of surfactant also influenced the composition of transition metal nanoparticles, as they have very high probability to form oxides in liquid environment. For the synthesis of copper (Cu) nanoparticles, CTAB or other surfactants have to be used otherwise formation of spindle-like Cu_2O/CuO structures are frequently observed [51, 52]. Change of composition of the nanoparticles from metal (Sn) to metal oxide (SnO_2) with discharge time even after the use of surfactant has also been reported by Lee et al. [21]. They explained the observation by investigating the pH of the solution. With the increase in discharge time for 50 mins, solution pH decreased i.e., H_2O_2 and HNO_3 were formed in the solution. HNO_3 may react with Sn to form SnO_2 nanoparticles as shown by the equation:

$$Sn + 4HNO_3 \rightarrow SnO_2 + 4NO_2(g) + 2H_2O \tag{26}$$

As HNO_3 was consumed during SnO_2 synthesis, the pH of the solution again increased for the discharge duration of 50 to 60 mins.

4. Conclusion

The main concern of this chapter is to deliver a general perception on the generation of plasma inside liquid and its importance in the field of material fabrication. In-Liquid Plasma method offers single-step, rapid and large-scale synthesis of uniform nanomaterials with different shapes, sizes and compositions. Moreover, from the economic point of view, it is a cost-effective approach as it does not require any gas, water cool vacuum chambers and pumping systems. Interaction of various reactive species on the synthesis of pure metal and metal oxide nanoparticles as well as nanocomposites has been discussed in this chapter. Morphological and compositional modification of nanomaterials by controlling the physical (e.g. applied voltage, current, pulse width and discharge duration) and chemical (e.g. solution concentration, pH and surfactant) parameters have also been discussed.

Author details

Palash Jyoti Boruah, Parismita Kalita and Heremba Bailung*
Plasma Application Laboratory, Physical Sciences Division, Institute of Advanced Study in Science and Technology (IASST), Guwahati, India

*Address all correspondence to: hbailung@yahoo.com

References

[1] Dou S, Tao L, Wang R, et al (2018) Plasma-Assisted Synthesis and Surface Modification of Electrode Materials for Renewable Energy. Adv Mater 30: 1705850. https://doi.org/10.1002/adma.201705850

[2] Bruggeman PJ, Kushner MJ, Locke BR, et al (2016) Plasma-liquid interactions: A review and roadmap. Plasma Sources Sci Technol 25:053002. https://doi.org/10.1088/0963-0252/25/5/053002

[3] Chen Q, Li J, Li Y (2015) A review of plasma-liquid interactions for nanomaterial synthesis. J Phys D Appl Phys 48:424005. https://doi.org/10.1088/0022-3727/48/42/424005

[4] Lukes P, Locke BR (2005) Plasmachemical oxidation processes in a hybrid gas-liquid electrical discharge reactor. J Phys D Appl Phys 38:4074–4081. https://doi.org/10.1088/0022-3727/38/22/010

[5] Ishigami M, Cumings J, Zettl A, Chen S (2000) A simple method for the continuous production of carbon nanotubes. Chem Phys Lett 319:457–459. https://doi.org/10.1016/S0009-2614(00)00151-2

[6] Sano N, Wang H, Chhowalla M, et al (2001) Synthesis of carbon 'onions' in water. Nature 414:506–507. https://doi.org/10.1038/35107141

[7] Zhu HW, Li XS, Jiang B, et al (2002) Formation of carbon nanotubes in water by the electric-arc technique. Chem Phys Lett 366:664–669. https://doi.org/10.1016/S0009-2614(02)01648-2

[8] Lange H, Sioda M, Huczko A, et al (2003) Nanocarbon production by arc discharge in water. Carbon N Y 41:1617–1623. https://doi.org/10.1016/S0008-6223(03)00111-8

[9] Sano N, Nakano J, Kanki T (2004) Synthesis of single-walled carbon nanotubes with nanohorns by arc in liquid nitrogen. Carbon N Y 42:686–691. https://doi.org/10.1016/j.carbon.2003.12.078

[10] Bera D, Kuiry SC, McCutchen M, et al (2004) In-situ synthesis of palladium nanoparticles-filled carbon nanotubes using arc-discharge in solution. Chem Phys Lett 386:364–368. https://doi.org/10.1016/j.cplett.2004.01.082

[11] Lo CH, Tsung TT, Chen LC (2005) Shape-controlled synthesis of Cu-based nanofluid using submerged arc nanoparticle synthesis system (SANSS). J Cryst Growth 277:636–642. https://doi.org/10.1016/j.jcrysgro.2005.01.067

[12] Lo CH, Tsung TT, Lin HM (2007) Preparation of silver nanofluid by the submerged arc nanoparticle synthesis system (SANSS). J Alloys Compd 434–435:659–662. https://doi.org/10.1016/j.jallcom.2006.08.217

[13] Lung JK, Huang JC, Tien DC, et al (2007) Preparation of gold nanoparticles by arc discharge in water. J Alloys Compd 434–435:655–658. https://doi.org/10.1016/j.jallcom.2006.08.213

[14] Ashkarran AA, Zad AI, Ahadian MM, Ardakani SAM (2008) Synthesis and photocatalytic activity of WO3 nanoparticles prepared by the arc discharge method in deionized water. Nanotechnology 19:195709. https://doi.org/10.1088/0957-4484/19/19/195709

[15] Ashkarran AA, Iraji zad A, Mahdavi SM, Ahadian MM (2009) ZnO nanoparticles prepared by electrical arc discharge method in water. Mater Chem Phys 118:6–8. https://doi.org/10.1016/j.matchemphys.2009.07.002

[16] Ashkarran AA, Afshar SAA, Aghigh SM, kavianipour M (2010) Photocatalytic activity of ZrO2 nanoparticles prepared by electrical arc discharge method in water. Polyhedron 29:1370–1374. https://doi.org/10.1016/j.poly.2010.01.003

[17] Omurzak E, Mashimo T, Iwamoto C, et al (2009) Synthesis of blue amorphous TiO 2 and Ti nO 2n-1 by the impulse plasma in liquid. J Nanosci Nanotechnol 9:6372–6375. https://doi.org/10.1166/jnn.2009.1331

[18] Saito N, Hieda J, Takai O (2009) Synthesis process of gold nanoparticles in solution plasma. Thin Solid Films 518:912–917. https://doi.org/10.1016/j.tsf.2009.07.156

[19] Pootawang P, Saito N, Takai O, Lee SY (2012) Synthesis and characteristics of Ag/Pt bimetallic nanocomposites by arc-discharge solution plasma processing. Nanotechnology 23:395602. https://doi.org/10.1088/0957-4484/23/39/395602

[20] Hattori Y, Nomura S, Mukasa S, et al (2013) Synthesis of tungsten oxide, silver, and gold nanoparticles by radio frequency plasma in water. J Alloys Compd 578:148–152. https://doi.org/10.1016/j.jallcom.2013.05.032

[21] Lee H, Park SH, Kim SJ, et al (2014) Synthesis of tin and tin oxide nanoparticles using liquid phase plasma in an aqueous solution. Microelectron Eng 126:153–157. https://doi.org/10.1016/j.mee.2014.07.014

[22] Lee H, Park SH, Kim SJ, et al (2015) Synthesis of manganese oxide/activated carbon composites for supercapacitor application using a liquid phase plasma reduction system. Int J Hydrogen Energy 40:754–759. https://doi.org/10.1016/j.ijhydene.2014.08.085

[23] Sun SH, Jung SC (2016) Facile synthesis of bimetallic Ni-Cu nanoparticles using liquid phase plasma method. Korean J Chem Eng 33:1075–1079. https://doi.org/10.1007/s11814-015-0262-0

[24] Panomsuwan G, Saito N, Ishizaki T (2016) Nitrogen-Doped Carbon Nanoparticle-Carbon Nanofiber Composite as an Efficient Metal-Free Cathode Catalyst for Oxygen Reduction Reaction. ACS Appl. Mater. Interfaces 8:6962–6971

[25] Ziashahabi A, Poursalehi R, Naseri N (2017) Formation mechanism of bead-chain-like ZnO nanostructures from oriented attachment of Zn/ZnO nanocomposites prepared via DC arc discharge in liquid. Mater Sci Semicond Process 72:128–133. https://doi.org/10.1016/j.mssp.2017.09.032

[26] Lee H, Lee WJ, Park YK, et al (2018) Liquid phase plasma synthesis of iron oxide nanoparticles on nitrogen-doped activated carbon resulting in nanocomposite for supercapacitor applications. Nanomaterials 8:190. https://doi.org/10.3390/nano8040190

[27] Yang B, Yu Y, Qiao J, et al (2020) Solution plasma method for the preparation of Cu-Ni/CuO-NiO with excellent methanol electrocatalytic oxidation performance. Appl Surf Sci 513:145808. https://doi.org/10.1016/j.apsusc.2020.145808

[28] Boruah PJ, Khanikar RR, Bailung H (2021) Novel single-step synthesis and shape transformation of Au/CuO micro/nanocomposites using plasma-liquid interaction. Nanotechnology 32:245601. https://doi.org/10.1088/1361-6528/abecb9

[29] Panomsuwan G, Watthanaphanit A, Ishizaki T, Saito N (2015) Water-plasma-assisted synthesis of black titania spheres with efficient visible-light photocatalytic activity. Phys Chem Chem Phys 17:13794–13799. https://doi.org/10.1039/c5cp00171d

[30] Pitchaimuthu S, Honda K, Suzuki S, et al (2018) Solution Plasma Process-Derived Defect-Induced Heterophase Anatase/Brookite TiO2 Nanocrystals for Enhanced Gaseous Photocatalytic Performance. ACS Omega 3:898–905. https://doi.org/10.1021/acsomega.7b01698

[31] Boruah PJ, Khanikar RR, Bailung H (2020) Synthesis and Characterization of Oxygen Vacancy Induced Narrow Bandgap Tungsten Oxide (WO3−x) Nanoparticles by Plasma Discharge in Liquid and Its Photocatalytic Activity. Plasma Chem Plasma Process 40:1019–1036. https://doi.org/10.1007/s11090-020-10073-3

[32] Parkansky N, Glikman L, Beilis II, et al (2007) W-C electrode erosion in a pulsed arc submerged in liquid. Plasma Chem Plasma Process 27:789–797. https://doi.org/10.1007/s11090-007-9099-6

[33] Yong Yang, Young I. Cho AF (2012) Plasma Discharge in Liquid: Water Treatment and Applications. CRC Press, Taylor & Francis Group, New York

[34] Fridman A, Gutsol A, Cho YI (2007) Non-thermal atmospheric pressure plasma. Adv Heat Transf 40:1–142. https://doi.org/10.1016/S0065-2717(07)40001-6

[35] Lun Li HO, Kang J, Urashima K, Saito N (2013) Comparison between the Mechanism of Liquid Plasma Discharge Process in Water and Organic Solution. J Inst Electrostat Jpn 37:22–27

[36] Hussein RO, Nie X, Northwood DO, et al (2010) Spectroscopic study of electrolytic plasma and discharging behaviour during the plasma electrolytic oxidation (PEO) process. J Phys D Appl Phys 43:105203. https://doi.org/10.1088/0022-3727/43/10/105203

[37] Klapkiv MD, Nykyforchyn HM, Posuvailo VM (1995) Spectral analysis of an electrolytic plasma in the process of synthesis of aluminum oxide. Mater Sci 30:333–343. https://doi.org/10.1007/BF00569685

[38] Dunleavy CS, Golosnoy IO, Curran JA, Clyne TW (2009) Characterisation of discharge events during plasma electrolytic oxidation. Surf Coatings Technol 203:3410–3419. https://doi.org/10.1016/j.surfcoat.2009.05.004

[39] Wu J, Zhang Y, Liu R, et al (2015) Anti-corrosion layer prepared by plasma electrolytic carbonitriding on pure aluminum. Appl Surf Sci 347:673–678. https://doi.org/10.1016/j.apsusc.2015.04.171

[40] Ashkarran AA, Iraji zad A, Mahdavi SM, et al (2009) Rapid and efficient synthesis of colloidal gold nanoparticles by arc discharge method. Appl Phys A Mater Sci Process 96:423–428. https://doi.org/10.1007/s00339-009-5288-x

[41] Bratescu MA, Cho SP, Takai O, Saito N (2011) Size-controlled gold nanoparticles synthesized in solution plasma. J Phys Chem C 115:24569–24576. https://doi.org/10.1021/jp207447c

[42] Klapkiv MD (1999) Simulation of synthesis of oxide-ceramic coatings in discharge channels of a metal-electrolyte system. Mater Sci 35:279–283. https://doi.org/10.1007/BF02359992

[43] Lu Q, Wang X, Yu J, et al (2020) Synthesis of spindle-like CuO nanoparticles by using cathode glow discharge electrolysis plasma. Mater Lett 264:127316. https://doi.org/10.1016/j.matlet.2020.127316

[44] Saito G, Hosokai S, Tsubota M, Akiyama T (2011) Synthesis of copper/copper oxide nanoparticles by solution plasma. J Appl Phys 110:023302. https://doi.org/10.1063/1.3610496

[45] Jin S, Kim S-M, Lee S, Kim J (2014) Synthesis and characterization of silver nanoparticles using a solution plasma process. J Nanosci Nanotechnol 14: 8094–8097. https://doi.org/10.1166/jnn.2014.9428

[46] Goree J (1994) Charging of particles in a plasma. Plasma Sources Sci Technol 3:400–406. https://doi.org/10.1088/0963-0252/3/3/025

[47] Kang J, Li OL, Saito N (2013) Synthesis of structure-controlled carbon nano spheres by solution plasma process. Carbon N Y 60:292–298. https://doi.org/10.1016/j.carbon.2013.04.040

[48] Goia D V., Matijević E (1999) Tailoring the particle size of monodispersed colloidal gold. Colloids Surfaces A Physicochem Eng Asp 146: 139–152. https://doi.org/10.1016/S0927-7757(98)00790-0

[49] Kim SM, Kim GS, Lee SY (2008) Effects of PVP and KCl concentrations on the synthesis of gold nanoparticles using a solution plasma processing. Mater Lett 62:4354–4356. https://doi.org/10.1016/j.matlet.2008.07.025

[50] Lee H, Chung M, Ahn HG, et al (2015) Effect of the surfactant on size of nickel nanoparticles generated by liquid-phase plasma method. Int J Precis Eng Manuf 16:1305–1310. https://doi.org/10.1007/s12541-015-0170-6

[51] Xie SY, Ma ZJ, Wang CF, et al (2004) Preparation and self-assembly of copper nanoparticles via discharge of copper rod electrodes in a surfactant solution: A combination of physical and chemical processes. J Solid State Chem 177:3743–3747. https://doi.org/10.1016/j.jssc.2004.07.012

[52] Yao WT, Yu SH, Zhou Y, et al (2005) Formation of uniform CuO nanorods by spontaneous aggregation: Selective synthesis of CuO, Cu 2 O, and Cu nanoparticles by a solid-liquid phase arc discharge process. J Phys Chem B 109:14011–14016. https://doi.org/10.1021/jp0517605